TU Delft
FACULTY OF MECHANICAL, MARITIME AND MATERIALS ENGINEERING
BIOMEDICAL ENGINEERING

MASTER OF SCIENCE THESIS

Identification of a two pivot human neck model using linear anterior-posterior perturbations

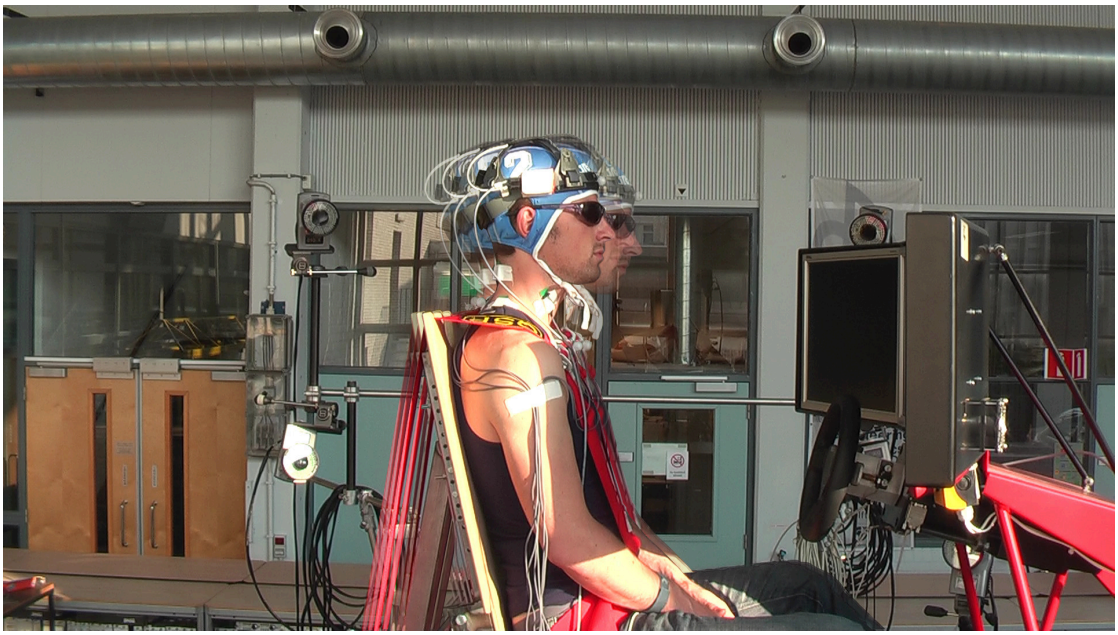

Paul van Drunen
December 2009

Title:
Identification of a two pivot human neck model using linear anterior-posterior perturbations

Type of report:
Master of Science Thesis

Author:
Paul van Drunen

Student Number:
1151169

Graduation Date:
2 December 2009

Institute:
Delft University of Technology
Faculty of Mechanical, Maritime and Materials Engineering
Department of BioMedical Engineering

Board of Examiners:
Prof. Dr. F.C.T. van der Helm (3mE, BMechE)
Dr. Ir. R. Happee (3mE, BMechE)
Dr. Ir. A.C. Schouten (3mE, BMechE)
P.A. Forbes, MASc (3mE, BMechE)
Dr. Ir. M.M. van Paassen (L&R, Control & Simulation)

Preface

In your hands you will find the end product of my master thesis. Seven and a half years of studying mechanical and biomedical engineering are combined into one report. However the end result would have been very different if it was not for the help and the wide research experience of my supervisor Riender Happee. The sparring-sessions, extra hands performing the experiments and contribution to the analysis of Patrick Forbes were highly appreciated. Thanks for all the help.

I'd like to thank all eight volunteers/friends for being available as guinea pig in such short notice. Finally thanks to my friends and family, in particular my girlfriend Sophie Lotgering, for all offered help and patience.

Cheers,

Paul van Drunen
pvandrunen@gmail.com

Contents

Identification of a two pivot human neck model using linear anterior-posterior perturbations

Paul van Drunen, Patrick A. Forbes, Riender Happee

Department of BioMechanical Engineering, Faculty of Mechanical Engineering, Laboratory for Neuromuscular Control, Delft University of Technology, Mekelweg 2, 2628 CD Delft, The Netherlands

Abstract

Eight healthy young adult males seated in a rigid chair and restrained by a five point harness belt underwent anterior-posterior random appearing multisine perturbations with a frequency range of 0.3-20 Hz. Six different conditions were tested differentiating in maximum acceleration level ([1;2;4;8] m/s^2) and in task (mental arithmetic and blindfolded). The head and neck kinematics were captured by a Qualisys motion capture system and Xsens accelerometers. Muscle activity of the trapezius and sternocleidomastoid muscles was collected by a Delsys EMG system. A two pivot neck model was developed representing the head-neck kinematics separating upper and lower neck kinematics. The kinematics were described with an error margin of 2.5 % of the maximum range of motion of the head. The amount of neck deformation relative to the perturbation is expressed in gain and phase, the linearity is expressed in squared coherence. For the head-neck kinematics a significant ($P < 0.05$) increase in gain was found for decreasing acceleration levels, indicating non-linearity of the human reflexes and/or the passive neck mechanics. At lower frequencies, the mental arithmetic task resulted in a 9 % decrease of neck deformations ($P < 0.01$). At lower frequencies, blindfolding resulted in a 16 % increase of neck deformations ($P < 0.05$). The pivot rotations showed for low acceleration levels similar gain and phase characteristics for both the upper and lower pivot up to 3 Hz. Increasing acceleration levels resulted in a major decrease of relative upper neck deformations ($P < 0.05$) and an increase of relative lower neck deformations ($P < 0.01$), suggesting different control strategies for both pivots. For frequencies above approximately 5 Hz an increasing phase lag up to 180° for the upper pivot with respect to the lower pivot is found, indicating C-shaped neck bending for low frequencies and S-shaped neck bending for high frequencies. With the exception of the upper pivot response the squared coherence showed globally values above 0.5 between 1-12 Hz.

Key words: *Human Neck, Head Kinematics, Stabilization, Identification*

1. Introduction

Understanding the neuromuscular control of the human neck will be beneficial for the vehicle safety industry as well as for clinical reasons. In the vehicle safety industry, crash dummies and mathematical human models are used to predict the human neck dynamics and internal loadings. Implementation of neuromuscular neck control will improve the biofidelity of current dummies and models, however the required knowledge is lacking. Also the medical field struggles with the unknowns of the neck reflexes. For cervical dystonia, a syndrome characterized by sustained involuntary muscle contractions, the pathophysiology is only partly understood and gives clues for both abnormalities in the cortical and subcortical areas of the brain, but also for alterations in the spinal cord and peripheral nervous system. Better knowledge of the neuromuscular reflexes will lead to better diagnostics and treatment of such neck disorders.

The role of neck muscular activity has been studied extensively for rear, frontal and lateral impact. Simulations and analysis of experimental data with different instructions regarding muscle tension showed major effects in head-neck kinematics and internal loadings due to pretension/cocontraction and proprioceptive muscle reflexes (van der Horst, 2002; Ono et al., 2006).

For neck control, low level random perturbation studies illustrated the importance of the vestibulocollic reflexes (VCR) (Guitton et al., 1986; Keshner, 2003) and occulocollic reflexes (OCR) (Guitton et al., 1986; Peterka, 2002). Parametric analysis of the visco-elastic muscle properties (Fard et al., 2004; Simoneau et al., 2008) and proprioceptive reflexes (Pedrocchi and Ferrigno, 2004) resulted in quantitative results regarding neck stabilization, but are limited to a one degree of freedom (DoF) model. Peng (1996) developed a two DoF linear model combining visco-elastic muscle properties, proprioceptive reflexes and VCR in the sagittal plane using parameters from various sources.

Non-linear reflex behavior has been found when different instructions or perturbations (methods and levels) are applied (Tangorra et al., 2003; Keshner et al., 2004; Cenciarini and Peterka, 2006; Happee and van Drunen, 2009). This behavior is explained by a strategy change of humans for stabilizing the head by adapting to the applied stimulus and should be taken into account during the analysis of experimental results with extracted reflex systems (i.e. by blindfolding) or different perturbation methods.

Earlier studies on the arm and the ankle showed that reflexive parameters as well as joint visco-elastic parameters could be uniquely identified using measurements combining kinematics and muscle activity (EMG) (van der Helm et al., 2002; de Vlugt et al., 2006; Schouten et al., 2008). The aim is to use this kind of measurements in combination with trunk and/or head loadings for the identification of the visco-elastic joint properties and proprioceptive, VCR and OCR reflexes.

This study presents the development of an experimental setup and a two pivot kinematic neck model for neuromuscular modeling during head stabilization in the sagittal plane. Volunteer experiments were performed with multisine perturbations in anterior-posterior direction by a motion platform. A two pivot neck model was developed representing the head kinematics with respect to the incisura jugularis at the top of the sternum. Finally non parametric frequency

analysis was performed evaluated for significant differences at the global head kinematics as well as the pivot rotations.

2. Experimental Methods

2.1. Subjects

Eight healthy male subjects with no self-reported history of physical injuries involving control of the head and neck (head, neck, upper-back, vestibular organs and eyes) participated in this study. Mean age, height and body mass ($\pm$ standard deviation) were 24 $\pm$ 3 years (range 20-28), 186 $\pm$ 8 cm and 84 $\pm$ 12 kg respectively. Each participant signed an informed consent form outlining the protocol.

2.2. Test apparatus and procedures

The subjects were seated in a rigid chair with a flat base and back and restrained by a five point harness belt. The seat base was horizontally oriented 0.3 *m* above the floor. The seat back was oriented ten degrees backwards, providing an 'automotive' passenger seating posture and allowing subjects to lean against the seat, providing continuous contact between the trunk and the chair (Figure 1). The seat was mounted on a six DoF motion platform, which was controlled by

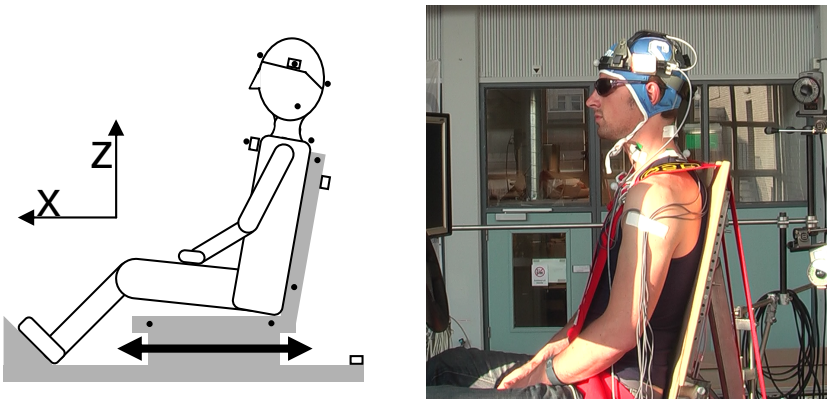

((a)) ((b))

Figure 1: *Schematic (a) and photo (b) of the experimental setup illustrating the posture of the subject during the experiments. The locations of the ten Qualisys markers (•) and four (the fifth is at the temple at the other side of the head) Xsens accelerometers (rectangular box) are shown. Sign conventions for the sled perturbation is the same as for the global coordinate system (X: anterior is positive, posterior is negative. Z: up is positive, down is negative) are given.*

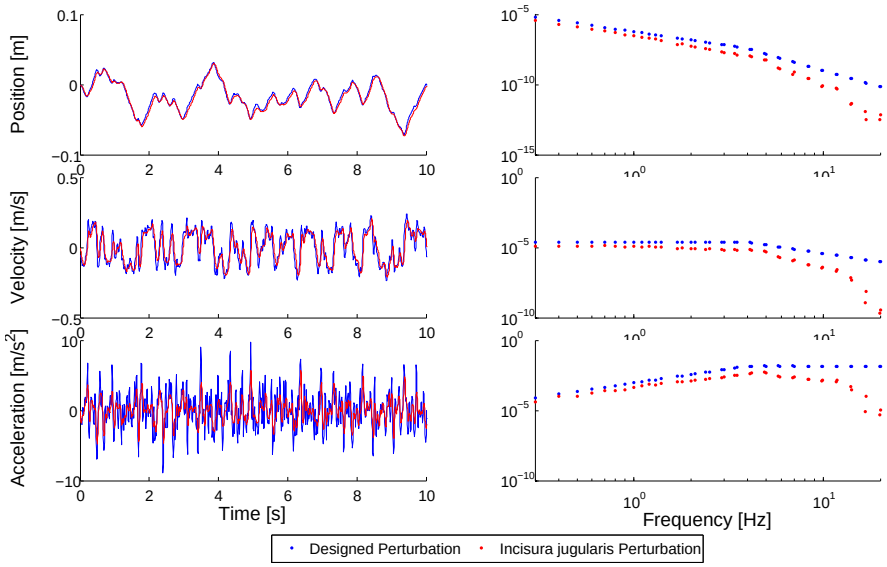

Figure 2: *Timetrace and autospectrum of the disturbance with a 8 m/s^2 peak acceleration. The designed perturbation as well as the resulting incisura jugularis (sternum) disturbance are given. See Appendix A for the explanation of the differences between designed and incisura jugularis perturbations. Left: The first 10 s of the disturbance timetrace. Right: Autospectrum.*

a dSpace[1] simulator system in combination with dSpace ControlDesk. For head measurements, the subjects wore a plastic, size-adjustable helmet attaching markers and accelerometers to the head. The weight of the entire helmet and attachments was 0.178 kg, which was considered negligible compared to the mass of the head (typically 4.5 kg).

The subjects were asked to tighten themselves to the chair using the restraint, maintaining a relaxed seating posture. Subjects were instructed to place their feet on a footrest, to bend their knees slightly, and to place their hands in their lap. Then they were instructed to place their head and neck in a comfortable and natural orientation, while focusing visually on a marker 5 m away at the approximate height of the subjects' eyes.

2.3. Stimuli

The motion platform was provided with a random appearing anterior-posterior perturbation (Figure 2) consisting of 42 sinusoids with frequencies between 0.3 and 20 Hz. Frequency averaging will reduce the variance of the spectral density. Therefore, every two adjacent sinusoids were paired by placing them close to each other at 0.05 Hz apart, resulting in 21 frequency pairs. The perturbation was designed with equal velocity amplitudes up to 4 Hz and appearing equal acceleration amplitudes from 4 to 20 Hz and was crested to a time-variable velocity signal for

[1] www.dspaceinc.com

optimized power (Schouten et al., 2008). Each run was comprised of a 10 s disturbance which was repeated once, resulting in a total runtime of 20 s. Four loading levels with 1, 2, 4 and 8 m/s^2 peak acceleration were tested five times in random order providing a total of twenty runs.

Additional tests were performed with the 8 m/s^2 peak acceleration disturbance for five runs where the subjects performed a mental arithmetic task to eliminate or reduce voluntary responses during the physical perturbations (Keshner, 2003). The mental arithmetic task contained a mathematical problem where fifteen summations or subtractions of integers below ten were given every 2 s, resulting in a total duration of 30 s (Vuillerme and Vincent, 2006).

Finally, five runs with the 8 m/s^2 peak acceleration disturbance were performed while the subjects were blindfolded to eliminate visual influences.

The entire experiment per subject took approximately 35 *min* excluding subject preparation.

2.4. Data collection

3D-displacements of the seat and the subjects were recorded using six infrared motion capture cameras (Qualisys[2] Oqus 3 series) at 200 frames per second. A total of nine markers were used to capture displacements throughout the whole test. Four markers were attached to the seat, three markers were attached to the helmet and two additional markers were attached directly to the subjects by using tape at the palpated incisura jugularis (IJ) at the upper sternum and directly below the mastoid process representing an estimate of the occipital condyle location.

Five Xsens[3] MTx sensors recorded the accelerations and rotational velocities of the platform, the backrest of the chair, the palpated incisura jugularis, and the left and right temple (attached to the helmet) at a rate of 64 Hz.

Electromyographic data was collected from the High Trapezius (TRH), the Low Trapezius (TRL) and the Sternocleidomastoid (SCM) muscles on both sides of the neck using a Delsys Bagnoli Desktop EMG System (www.delsys.com) connected to the Qualisys D/A converter at a rate of 3000 Hz. The Qualisys and Xsens systems were synchronized to one another by an external electric pulse applied to both systems.

3. Data analysis

As described in Appendix A the motion capture data provides a good coherence from 0.3 to 12 Hz, even after a double differentiation as needed to calculate accelerations and moments. Optimally the recorded motion capture and acceleration data could be merged using a Kalman

[2]www.qualisys.com
[3]www.xsens.com

filter, but given the apparent noise levels in the accelerations, only the motion capture data will be analyzed further.

Head motion was expressed in a head coordinate system having its origin in the head center of gravity (CG) and an x-axis in the Frankfurt plane (the plane passing through the inferior margin of the left orbit and the upper margin of each ear canal). Initial measurements of each subject were used to calculate the location of the head CG (by (Clauser et al., 1969)) and Frankfurt plane, such that the horizontal (X_{CG}) & vertical (Z_{CG}) translation and rotation (α) of the head could be calculated respectively.

3.1. Two pivot model

Flexion and extension motion of the neck utilizes seven joint connections between the cervical vertebrae. Therefore, the best method of representing the head motion would be to use a model having seven rigid bodies representing the cervical vertebrae and head connected via rotational joints. However, due to the complexity of such a model simplifications are preferred. A one pivot model (Fard et al., 2004; Pedrocchi and Ferrigno, 2004; Simoneau et al., 2008) has been found insufficient for describing the head motion in the sagittal plane, since during realistic head motion the head translations are separate from the head rotations. Previously developed two pivot models have however been shown to provide sufficient approximations of both the rotation and translation of the head (Wismans et al., 1987; Peng, 1996).

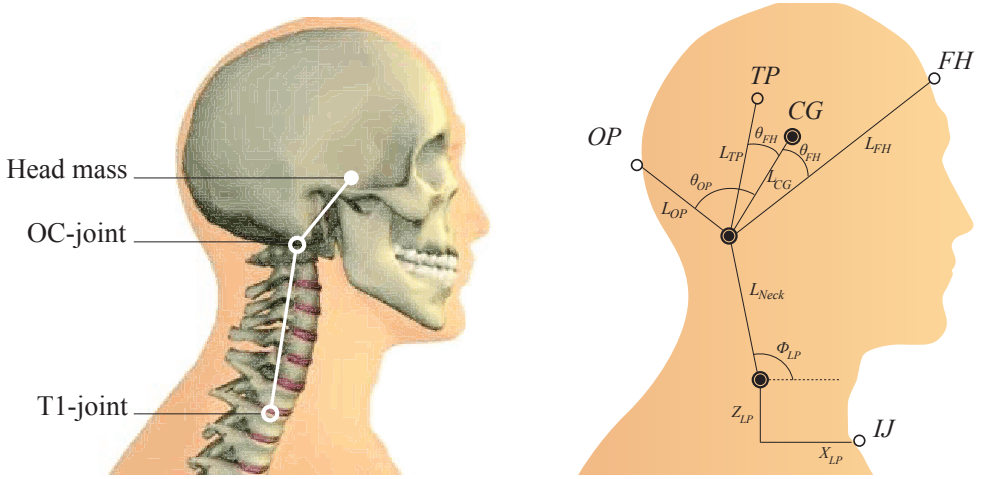

((a)) *The Human Head–Neck System with the schematic anthropometric pivots (○).*

((b)) *The two pivot model schematically including all geometric parameters. Markers are included (○) as well as the pivot points (●).*

Figure 3: *The Two Pivot Model*

Table 1
Geometric parameters estimated by the pivot optimization (Figure 3(b))

No.	Par.	Unit	Description
1	X_{LP}	[m]	Horizontal translation of lower pivot (LP) with respect to incisura jugularis (IJ)
2	Z_{LP}	[m]	Vertical translation of lower pivot with respect to incisura jugularis
3	L_{Neck}	[m]	Distance between the lower pivot and upper pivot (UP) representing the neck
4	L_{CG}	[m]	Distance between the upper pivot and the head center of gravity (CG)
5	L_{OP}	[m]	Distance between the upper pivot and the occiput (OP)
6	L_{FH}	[m]	Distance between the upper pivot and the forehead (FH)
7	L_{TP}	[m]	Distance between the upper pivot and the temple (TP)
8	θ_{OP}	[rad]	Angle between L_{CG} and L_{OP}
9	θ_{FH}	[rad]	Angle between L_{CG} and L_{FH}
10	θ_{TP}	[rad]	Angle between L_{CG} and L_{TP}
11	$\phi_{LP}(t)$	[rad]	Pivot rotation of the lower pivot
12	$\phi_{UP}(t)$	[rad]	Pivot rotation of the upper pivot

3.2. Pivot optimization

In previous two pivot modeling studies, the positions of the pivots were chosen anthropometrically with a lower pivot between the T1 and C7 vertebrae and an upper pivot at the approximate location of the occipital condyle (Figure 3(a)). The two pivot neck model is in fact a representation of an eight jointed human neck. Defining the pivots anthropometrically could result in a sufficient approximation, however this approximation is not necessarily optimal. Therefore, a pivot optimization was performed. The goal of this optimization was to obtain positions of the lower (LP) and upper pivot (UP) for each subject, which approximates the head rotation and translation optimally. The marker data of the incisura jugularis (IJ), the occiput (OP), the temple (TP) and the forehead (FH) were used for this optimization as well as the calculated head center of gravity (CG)).

Per subject, ten geometric parameters and the two pivot angles (Table 1 and Figure 3(b)) were optimized. The marker positions in the model were estimated with the two pivot model equations:

$$\hat{\mathbf{x}}_i = \mathbf{x}_{IJ} + \mathbf{x}_{LP} + L_{Neck} \cdot \mathbf{R}_{\phi_{LP}}(t) + L_i \cdot \mathbf{R}_{\phi_{UP}}(t) \cdot \mathbf{R}_{\theta_i} \tag{1}$$

where i is $\{CG, OP, FH, TP\}$, the $\mathbf{x}$ is the 2D-position vector $[X, Z]$ and $\mathbf{R}$ (Equation 2) is the rotation matrix around the different pivots, with θ_{CG} defined as zero. The hat denotes the estimate.

$$\mathbf{R}_q = \begin{bmatrix} \cos(q) & -\sin(q) \\ \sin(q) & \cos(q) \end{bmatrix} \tag{2}$$

The optimization is performed with a non-linear sum of least-squares method, using the *lsqnonlin* algorithm provided by matlab. The minimization criterion (Equation 3) is the summation of

the normalized head rotation error (Equation 4) and the normalized position error (Equation 5) of all three markers and the center of gravity:

$$V_N(P) = \frac{1}{N}\sum_{n=0}^{N}\left(\varepsilon_\alpha(n,P) + \sum_{i=1}^{4}\varepsilon_i(n,P)\right)^2 \tag{3}$$

where V_N is the quadratic function of the approximation error, N is the number of time samples, P the parameter vector and the error functions are:

$$\varepsilon_\alpha(n,P) = \frac{\hat{\alpha}(n,P) - \alpha(n)}{\Delta\alpha(n)} \tag{4}$$

$$\varepsilon_i(n,P) = \frac{\sqrt{(\hat{x}_i(n,P) - x_i(n))^2 + (\hat{z}_i(n,P) - z_i(n))^2}}{\sqrt{(\Delta x_i(n))^2 + (\Delta z_i(n))^2}} \tag{5}$$

where the Δ denotes the range of the variable within the experiment.

Due to computational limitations caused by optimizing the time variant two pivot angles, the motion capture data was first resampled from 200 to 50 Hz and then divided into parts of one second, resulting in $n_{runs} \cdot n_{parts/run} = 30 \cdot 20 = 600$ parts per subject. The per part optimized geometric parameters were averaged over all parts resulting in the final geometric parameter set for each subject. To derive the two pivot angle time vectors the data was re-analyzed with the final geometric parameters at 200 Hz.

3.3. Nonparametric frequency analysis

The time records of disturbance at the chair ($X_{CH}(t)$), the incisura jugularis ($X_{IJ}(t)$), the head ($X_{TP}(t)$, $Z_{TP}(t)$, and $\alpha(t)$) and the pivot rotations ($\phi_{LP}(t)$, and $\phi_{UP}(t)$) were analyzed. Each time record was divided into two parts of 10 s representing the repeated disturbance and transformed into the frequency domain using the fast Fourier transform (FFT). To reduce variance due to noise, the frequency spectra were averaged over the two parts as well as the five repetitions with the same condition. Because of interaction between the manipulator (the chair) and the subject, closed loop identification algorithms are required to estimate the frequency response functions (FRFs) between the incisura jugularis and the horizontal head displacements ($\hat{H}_{X_{TP}}(f)$), the vertical head displacements ($\hat{H}_{Z_{TP}}(f)$), the head rotations ($\hat{H}_\alpha(f)$), and the two pivot rotations ($\hat{H}_{\phi_{LP}}(f)$ & $\hat{H}_{\phi_{UP}}(f)$):

$$\hat{H}_q(f) = \frac{\hat{S}_{X_{CH},q}(f)}{\hat{S}_{X_{CH},X_{IJ}}(f)} \tag{6}$$

where q is $\{X_{TP}, Z_{TP}, \alpha, \phi_{LP}, \phi_{UP}\}$, and $\hat{S}_{X_{CH},qq}(f)$ is the estimated cross spectral density between X_{CH} and qq (hat denotes estimate). The FRF is a presented as a gain ($\mid H \mid$) and phase ($\angle H$) and represents the neck deformations. To reduce the variance of the spectral densities, averaging

was performed over the two paired frequencies (Mugge et al., 2007). Coherence is a measure of linearity between two different signals varying between 0 and 1 and decreasing due to non-linearity and noise. While in a later research stage a linear model will be developed for this results, high coherence is highly preferred. The coherence is estimated for the different signals by

$$\hat{\gamma}_q^2(f) = \frac{\mid \hat{S}_{X_{CH},q}(f) \mid^2}{\hat{S}_{X_{CH},X_{CH}}(f)\hat{S}_{q,q}(f)} \tag{7}$$

4. Results

4.1. Pivot optimization

The optimized geometric parameters, describing the subject specific models, are given in Table 2. The intrasubject variation (S.D.), a measure of parameters' performance for the total test set, is found for all subjects between 1-12 % of the optimized parameters with a maximum variation of 3.25 *mm* in position and 0.02 *rad* in orientation. The anthropometric differences are shown by the intersubject variation between 5-20 % of the average. The final optimization errors (Equations 4 & 5) are given in Table 3. For all subjects the mean error is within 2.5 % of the total motion range. Figure 4 shows an example of the final fit of the recorded kinematics, where the model kinematics are traced on top of the experimental kinematics.

Table 2
Estimated geometric parameters (mean(±S.D.)) for all subjects and the average (mean(±S.D.)) across all subjects.

		Value (mean(±S.D.))								
Parameter		Subject 1	Subject 2	Subject 3	Subject 4	Subject 5	Subject 6	Subject 7	Subject 8	Average
X_{LP}	[*mm*]	-87.44(1.51)	-91.74(0.82)	-82.58(1.00)	-81.94(1.49)	-81.11(0.71)	-78.70(2.49)	-78.66(1.08)	-88.04(1.04)	-83.78(4.76)
Z_{LP}	[*mm*]	18.70(2.06)	19.60(1.34)	23.73(1.25)	16.53(1.92)	23.51(1.61)	21.97(1.27)	29.06(1.91)	27.95(1.15)	22.63(4.37)
L_{Neck}	[*mm*]	109.58(1.95)	112.67(1.47)	126.18(1.03)	118.99(1.35)	114.10(1.81)	128.86(1.37)	137.53(1.88)	135.04(1.50)	122.87(10.57)
L_{CG}	[*mm*]	84.29(3.25)	65.71(2.98)	99.97(2.41)	113.85(2.12)	91.64(2.56)	94.18(2.51)	106.44(1.93)	111.70(2.33)	95.97(15.89)
L_{OP}	[*mm*]	94.35(1.86)	110.62(1.26)	108.63(0.49)	103.47(1.37)	95.85(1.76)	122.81(1.29)	112.93(1.96)	98.62(1.65)	105.91(9.70)
L_{FH}	[*mm*]	196.65(3.13)	186.95(2.53)	204.00(2.25)	219.84(2.07)	194.48(1.99)	201.36(1.91)	205.95(1.61)	207.57(2.29)	202.10(9.86)
L_{TP}	[*mm*]	142.15(3.22)	132.60(3.07)	142.94(2.46)	151.29(2.15)	119.40(2.63)	147.14(2.38)	154.89(2.03)	149.05(2.65)	142.43(11.51)
θ_{OP}	[*rad*]	1.44(0.03)	1.38(0.02)	1.24(0.02)	1.21(0.02)	1.22(0.02)	1.12(0.02)	1.11(0.01)	1.15(0.02)	1.23(0.12)
θ_{FH}	[*rad*]	-0.54(0.02)	-0.67(0.02)	-0.55(0.01)	-0.43(0.01)	-0.68(0.02)	-0.64(0.01)	-0.64(0.01)	-0.69(0.02)	-0.61(0.09)
θ_{TP}	[*rad*]	-0.03(0.01)	-0.14(0.02)	-0.01(0.00)	0.04(0.00)	-0.14(0.01)	-0.15(0.01)	-0.16(0.01)	-0.22(0.01)	-0.10(0.09)

Table 3
Estimated normalized errors (mean(±S.D.)) for all subjects and the average (mean(±S.D.)) accross all subjects. The error values are percentages of the total range of motion of the particular marker data.

		Value (mean(±S.D.))								
Error		Subject 1	Subject 2	Subject 3	Subject 4	Subject 5	Subject 6	Subject 7	Subject 8	Average
ε_{CG}	[%]	1.69(0.03)	1.58(0.04)	2.12(0.06)	1.86(0.05)	1.26(0.04)	1.16(0.03)	1.70(0.03)	0.95(0.03)	1.54(0.39)
ε_{OC}	[%]	2.18(0.04)	1.44(0.05)	2.48(0.06)	1.89(0.04)	1.43(0.04)	1.37(0.03)	1.78(0.03)	1.22(0.04)	1.72(0.44)
ε_{FH}	[%]	0.87(0.01)	1.30(0.01)	1.14(0.01)	1.32(0.01)	1.00(0.02)	0.87(0.01)	0.99(0.01)	0.68(0.01)	1.02(0.22)
ε_{TP}	[%]	1.65(0.03)	1.60(0.04)	2.27(0.03)	4.58(0.07)	1.61(0.03)	1.98(0.02)	1.47(0.02)	1.69(0.02)	2.11(1.03)
ε_{α}	[%]	0.08(0.01)	0.04(0.01)	0.08(0.01)	0.06(0.01)	0.07(0.01)	0.06(0.01)	0.05(0.01)	0.10(0.01)	0.07(0.02)

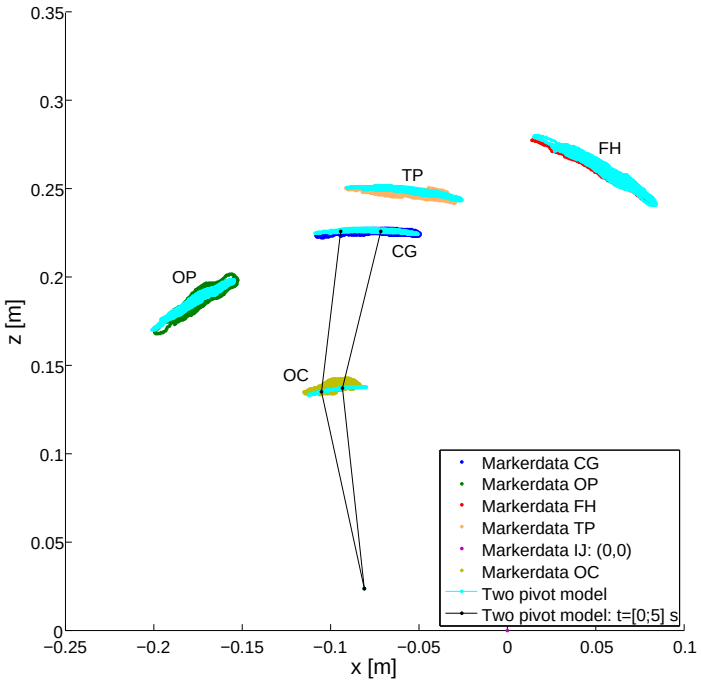

((a)) *Trajectory in the sagittal plane*

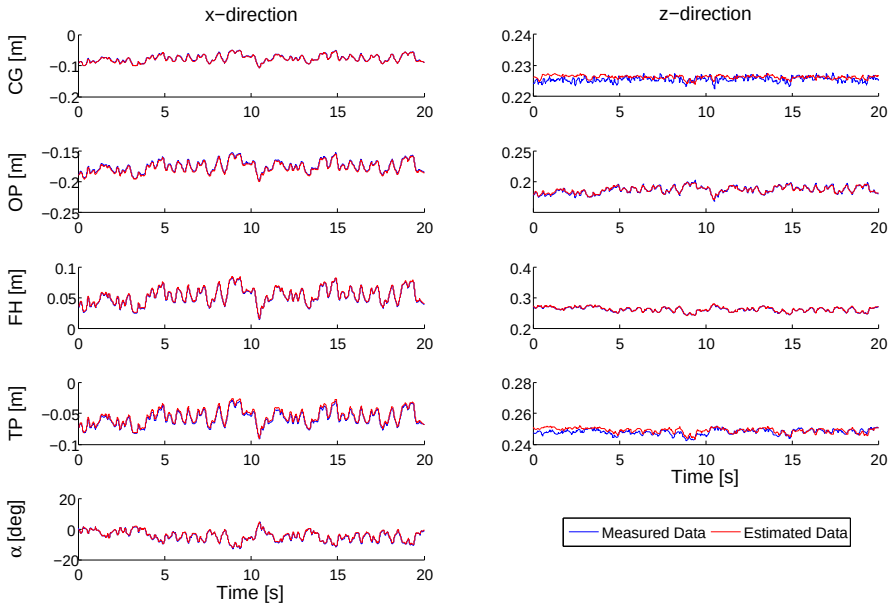

((b)) *Time history in horizontal (x) and vertical (z) direction*

Figure 4: *An example of the pivot optimization results of subject 5 at 8 m/s^2. The marker data (Head center of gravity (CG), Occiput (OP), Forehead (FH), Temple (TP), Incisura Jugularis (IJ) and palpated Occipital Condyle (OC) with respect to the incisura jugularis against the two pivot model representation of the markers.*

4.2. Head-neck kinematics

The head-neck kinematics were investigated in the frequency domain. Therefore, nonparametric frequency analysis was done for the global head horizontal displacement ($\hat{H}_{X_{TP}}(f)$), rotations ($\hat{H}_{\alpha}(f)$), as well as for the two pivot model rotations ($\hat{H}_{\phi_{LP}}(f)$ & $\hat{H}_{\phi_{UP}}(f)$). The gain, phase and coherence characteristics of these estimated FRFs are given in Figure 5 (global head horizontal displacement and rotations) and Figure 6 (pivot rotations) for all six conditions, averaged over all subjects and runs. The gain and phase are defined as the neck deformations relative to the perturbation, while squared coherence gives a measure of linearity.

The graphs show marked differences between conditions. To check the magnitude and significance of these differences a two-tailed paired Student T-test was performed on the gain (Table 4), phase and coherence (Appendix C) characteristics for all subjects during the different conditions with respect to the 8 m/s^2 condition. The analysis was split up into the following frequency ranges in order to provide a partitioned and more detailed analysis of the data:

FR1: $0.3 - 0.8 \;\; Hz$
FR2: $0.8 - 3.0 \;\; Hz$
FR3: $3.0 - 7.0 \;\; Hz$
FR4: $7.0 - 12.0\, Hz$

The global head displacement and rotation show a significant gain increase for lower acceleration levels in all frequency ranges (Figure 5). This suggests a non-linear human response with higher relative neck deformations at lower perturbation levels. At frequencies between 0.8-3 Hz the highest increase of relatively neck deformations are found in particular with the lower perturbation levels . Mental distraction leads to a significant ($P < 0.01$) gain decrease at low frequencies ($< 3\ Hz$), while excluding the visual contribution by blindfolding leads to a significant ($P < 0.05$) gain increase at low frequencies ($< 3\ Hz$). This is thought to be a result of the visual and voluntary feedback having only low frequency contribution.

Pivot rotations measured at the two locations show different responses (Figure 6). The lower pivot shows significant ($P < 0.05$) gain decrease for decreasing perturbation levels up to 7 Hz and therefore lower relative neck deformations. On the other hand the upper pivot shows very large significant ($P < 0.01$) gain increase for decreasing perturbation levels up to 7 Hz, resulting in an increase of relative neck deformations for lower perturbation levels. For the lower pivot only in FR2 did the mental distraction condition result in a significant ($P < 0.001$) decrease in gain and the upper pivot showed higher gain ($P < 0.05$). After excluding the visual contribution significant ($P < 0.05$) reductions in relative neck rotations are found between 0.8 and 7 Hz in both pivots.

Table 4
Significant mean value differences of the gain $|H|$ from the incisura jugularis horizontal displacement to the horizontal head displacement (upper-left), the head angle (upper-right), the lower pivot angle (lower-left) and the upper pivot angle (lower-right). $|H|$ is compared with the $8 m/s^2$ disturbance level within four different frequency ranges. For phase and coherence significances and the detailed p-values see Appendix C.

		$\lvert \hat{H} \rvert_{X_{TP}}$				$\lvert \hat{H} \rvert_{\alpha}$			
Perturbation level		0-0.8 Hz	0.8-3 Hz	3-7 Hz	7-12 Hz	0-0.8 Hz	0.8-3 Hz	3-7 Hz	7-12 Hz
1 m/s^2	[−]	1.099[3]	1.341[3]	1.311[3]	1.727[3]		1.471[3]	1.206[3]	1.205[3]
2 m/s^2	[−]	1.044[1]	1.223[3]	1.151[1]	1.370[2]		1.376[3]	1.201[3]	1.090[1]
4 m/s^2	[−]		1.082[2]				1.174[3]	1.133[3]	
MentalArithmetic	[−]	0.944[2]	0.901[3]				0.875[2]		
EyesClosed	[−]	1.172[3]				1.159[2]	1.100[1]		
		$\lvert \hat{H} \rvert_{\phi_{LP}}$				$\lvert \hat{H} \rvert_{\phi_{UP}}$			
		0-0.8 Hz	0.8-3 Hz	3-7 Hz	7-12 Hz	0-0.8 Hz	0.8-3 Hz	3-7 Hz	7-12 Hz
1 m/s^2	[−]	0.764[3]	0.918[1]	0.867[1]		2.354[3]	2.342[3]	1.330[3]	
2 m/s^2	[−]	0.770[3]	0.908[1]			1.729[3]	2.095[3]	1.373[3]	
4 m/s^2	[−]	0.833[2]	0.916[1]			1.258[2]	1.487[3]	1.269[3]	
MentalArithmetic	[−]		0.810[3]				1.209[1]		
EyesClosed	[−]			1.121[1]			1.352[3]	1.176[1]	

[1] Significance p≤5.0%
[2] Significance p≤1.0%
[3] Significance p≤0.1%

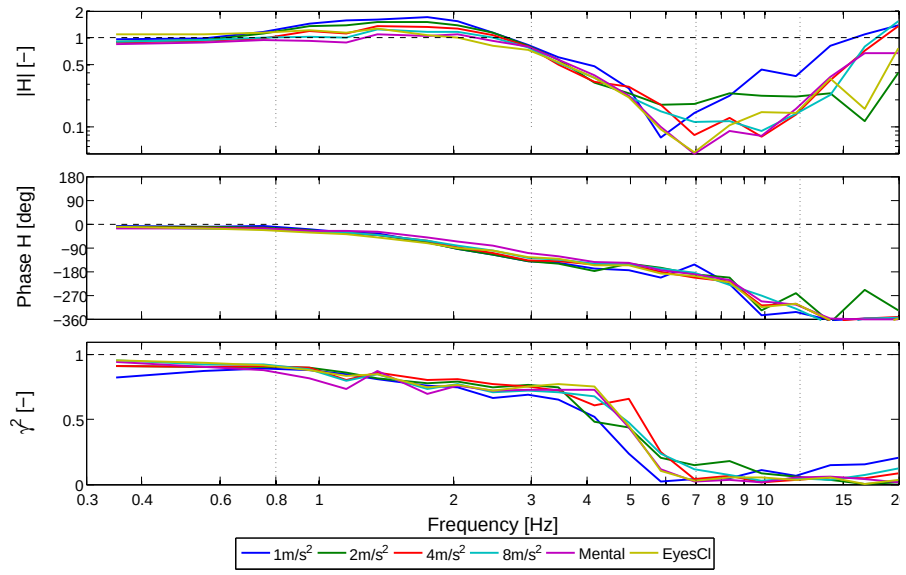

((a))

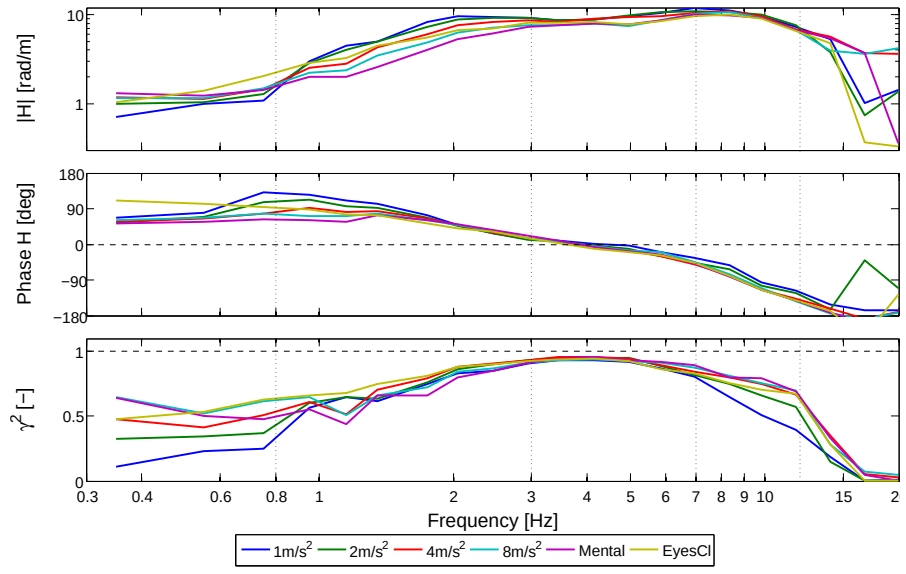

((b))

Figure 5: *Gain, Phase & Squared Coherence of the global head horizontal displacement (X_{TP}) and head rotation (α) with respect to the horizontal incisura jugularis displacements (X_{IJ}). All six different conditions ([1;2;4;8] m/s^2, Mental Arithmetic & Eyes Closed) are shown. The four different frequency ranges are marked by the vertical dotted lines.*
a: $\hat{H}_{X_{TP}}$, Transfer for horizontal incisura jugularis disturbance to horizontal temple (head) displacement
b: $\hat{H}_{\alpha}$, Transfer for horizontal incisura jugularis disturbance to head rotations

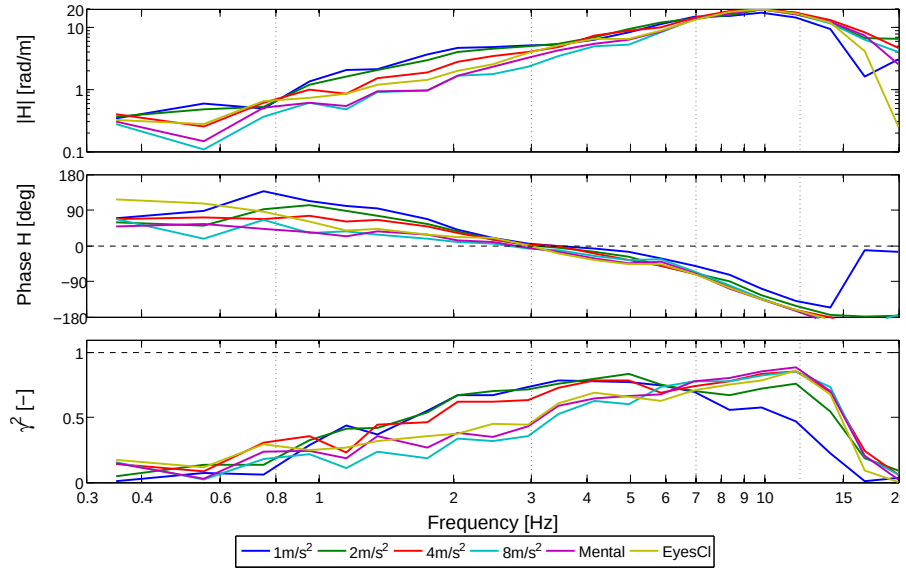

((a))

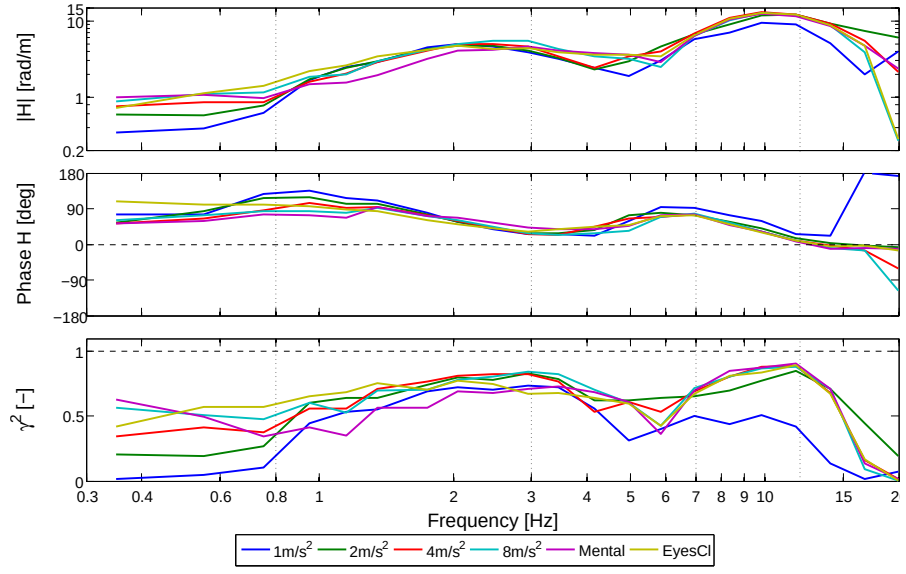

((b))

Figure 6: *Gain, Phase & Squared Coherence of the model pivot angles (ϕ_{LP}&ϕ_{UP}) with respect to the horizontal incisura jugularis displacements (X_{IJ}). All six different conditions ([1;2;4;8] m/s^2, Mental Arithmetic & Eyes Closed) are shown. The four different frequency ranges are marked by the vertical dotted lines.*
a: $\hat{H}_{\phi_{UP}}$, Transfer for horizontal incisura jugularis disturbance to upper pivot rotations
b: $\hat{H}_{\phi_{LP}}$, Transfer for horizontal incisura jugularis disturbance to lower pivot rotations

5. Discussion

This study presents the development of an experimental setup and a two pivot kinematic neck model for neuromuscular modeling during head stabilization in the sagittal plane. Volunteer experiments were performed with multisine perturbations in anterior-posterior direction by a six DoF motion platform. A two pivot neck model was developed representing the head kinematics with respect to the incisura jugularis at the top of the sternum. For the global head kinematics as well as for the pivot rotations non parametric frequency analysis was performed and evaluated for significant differences between the six perturbation conditions.

5.1. Experimental setup and protocol

The experiments were evaluated regarding the transfer of the designed perturbation to the incisura jugularis, the quality of the available data (Appendix A) and the frequency response functions of the neck and head (Appendix B and Results).

Figure 2 shows that at the lower frequencies the incisura jugularis (sternum) adequately follows the designed perturbations while at higher frequencies the incisura jugularis perturbation is highly reduced. These differences have been evaluated for the performance of three subsystems: (1) the designed perturbation to platform response, (2) the platform to seat response, and (3) the seat to incisura jugularis response. The platform did not replicate the designed perturbation at high frequencies (Figure 9(a)), due to a rate limiter and saturation (at 0.25 m/s and 0.14 m) applied to the hydraulic pistons of the platform. The response of the seat to the platform perturbations increased for high frequencies (Figure 9(b)), indicating insufficient stiffness of the seat. The seat to incisura jugularis transmission showed very good results, i.e. a gain close to 1 up to at least 12 Hz (Figure 10), indicating that the seat to body contact and restraint by the seat belt are sufficient. These three responses suggest that improvements to the platform and chair are needed to ensure true transfer of a 20 Hz designed perturbation to the neck. Nonetheless, the data gathered in this study remains valid, since the coherence and thus signal-to-noise ratio are high for frequencies up to 12 Hz.

A comparison of the accelerometer and the double differentiated motion capture data showed very comparable output from the two different measurements systems (Figures 10 & 11). Differences were found at the incisura jugularis data only for low frequencies (< 1 Hz), where a gain and coherence drop was found for the accelerometer data. This was thought to be due to natural respiration of the subjects. Ideally, a Kalman filter should be used to merge the two datasets together; however, due to the similarity of the two data sources no big improvements were to be expected. Also due to the good results of the motion capture and the appearing noise at the accelerometer data, only motion capture was analyzed further in this study.

The frequency response functions of the head and neck to the perturbations were evaluated globally (Figure 5) and locally (Figure 12). High squared coherence values are important for linear neuromuscular modeling. For the head rotation (Figure 5(b)) and the local horizontal head trans-

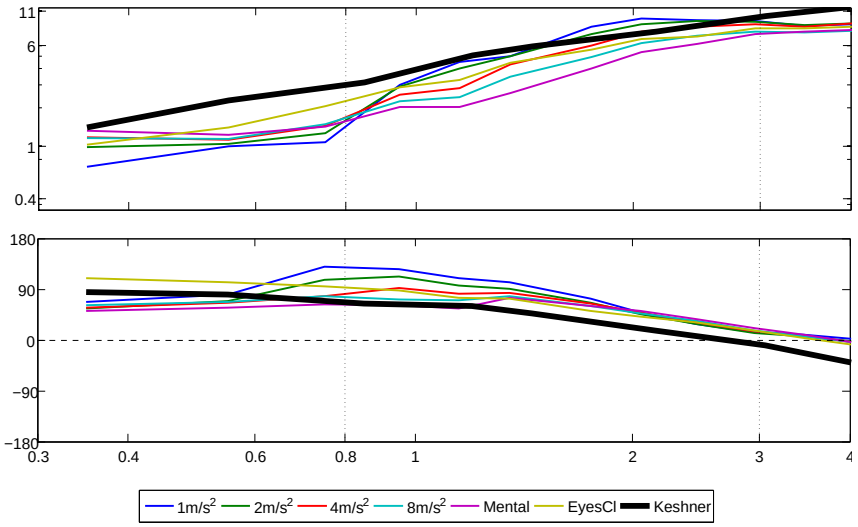

Figure 7: *The gain and phase characteristics of the head rotations of Keshner (2003) and presented in this study (Figure 5(b)).*

lation (Figure 12(b)) the squared coherence characteristics were comparable and globally above 0.5 for all six conditions at frequencies between approximately 1-12 Hz. High acceleration levels (4 & 8 m/s^2) even resulted in squared coherence levels above 0.5 at low frequencies. For low acceleration levels the squared coherence seem to be rather small, presumably due to the signal to noise ratio. On the other hand Tables 4 & 5 show that gain and phase depend strongly and significantly on the applied perturbation level indicating a non-linear behavior, which may also explain the somewhat low coherence values found. The mental arithmetic and eyes closed conditions were performed for improvement of the coherence at low frequencies (Keshner, 2000), however no significant coherence change has been found.

The low gains for the vertical head translation (Figure 12(a)) suggest that the occupants were loaded in a primarily horizontal direction, i.e. the intended objective of these tests.

The FRFs of the local horizontal head translation and the head rotation showed lower gains up to approximately 3 Hz, suggesting that muscular feedback effectively reduces head motion at these frequencies.. Comparison of the experimental results for head rotations in this study with earlier research with similar experimental protocol showed a high level of correspondence. Keshner (2003) presented the FRF of horizontal anterior-posterior perturbations to the head rotations for healthy subjects, resulting in comparable gain and phase characteristics at frequencies below 4 Hz (Figure 7).

A recent study also found comparable gain and phase characteristics for head rotations (Tangorra et al., 2003). However these experiments were performed with a rotational head perturbator in the horizontal plane and resulted in higher squared coherence at lower frequencies. This suggests better coherence for head perturbations and therefore a possible improvement of the

recent experimental setup. The coherence increase is possibly due to the direct nature of head perturbations to the head-neck system.

Although not documented in this study, a brief examination of the EMG (muscle activity) responses showed coherence > 0.5, suggesting the measurements to be sufficient for analysis and further neuromuscular modeling.

5.2. Two pivot neck kinematics

Neuromuscular analysis of the neck requires a geometric neck model representing global neck joints with surrounding muscles as torque generators. In previous studies two pivot neck models separating the upper and lower neck kinematics have shown to provide sufficient approximations of the head translations and rotations (Wismans et al., 1987; Peng, 1996). However, the numerical optimization of the neck geometry is a unique improvement over the previous anthropometrically estimated geometries. The results show very good head motion estimations with small errors ($< 2.5\%$ of the total range of motion), which is also presented in Figures 4(a) & 4(b) and Tables 2 & 3. The accuracy of the geometric parameters was defined by the intrasubject standard deviation and contains the potentially different neck posture during different experimental runs and the variance of the parameters. The intrasubject standard deviations were very low ($< 12\%$ of the mean) which implies a good fit with constant results.

The pivot positions defined by the numerical optimized two pivot neck model are compared to the anthropometrically defined pivot positions. The upper pivot was estimated close to the occipital condyle joint, representing the upper pivot for the anthropometric pivot model. However, the lower pivot was found slightly shifted frontally with respect to the anthropomorphically defined joint between the vertebral disks T1 and C7. This behavior could be explained by the ability of the human neck to bend, since a real human neck consists of eight neck joints. In the two pivot neck model the neck is presented as a rigid bar and so anthropometric defined pivots do not represent neck bending, while numerical optimized pivots do.

In defining the head center of gravity for each subject separately the Clauser method (Clauser et al., 1969) appeared to place its location more rearward as compared to previous modeling efforts (Plaga et al., 2005) and requires extra research for future experiments.

5.3. Pivot responses and stabilizing strategies

Humans control their joint motion by muscle contractions. Therefore, the frequency response functions of the pivot rotations give a representation of neck stabilization characteristics of humans (Figure 6). For the upper pivot, a low squared coherence is found at low frequencies especially for the highest acceleration amplitudes, indicating high non-linearity likely caused by non-linear passive neck mechanics and/or reflexes of the upper neck. The lower pivot showed reasonable coherence (> 0.4) for the higher acceleration amplitudes (4 & 8 m/s^2), while the

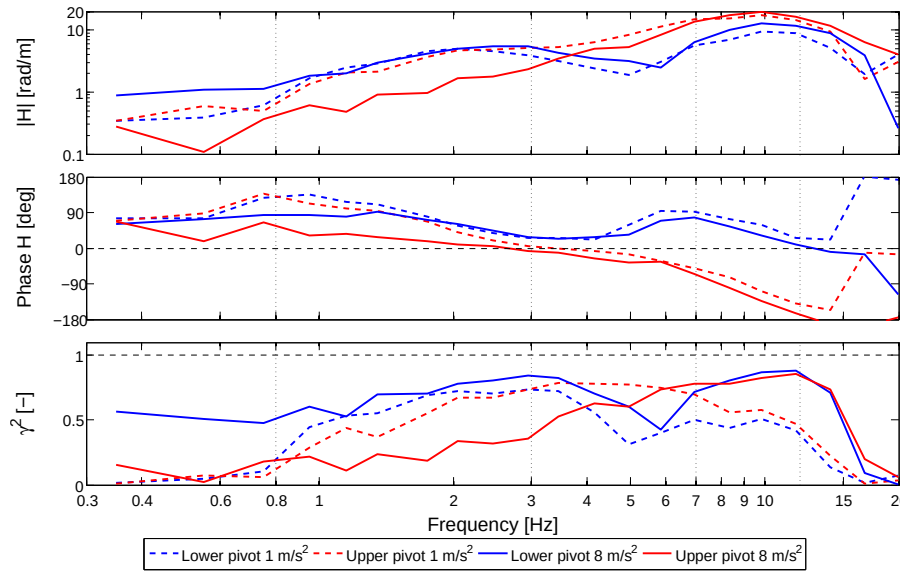

Figure 8: *Gain, Phase & Squared Coherence of the lower and upper pivot angles (ϕ_{LP}&ϕ_{UP}) with respect to the horizontal incisura jugularis displacements (X_{IJ}) with 1 & 8 m/s^2 acceleration level. The four different frequency ranges are marked by the vertical dotted lines. Other conditions can be found for separate pivots in Figure 6.*

lower acceleration amplitudes showed at low frequencies very low coherence. The increasing gain for both pivots describes increased relative pivot rotation responses at higher frequencies.

Remarkable results were observed in the gain and phase characteristics of the upper and lower pivots (Figure 8). Low acceleration perturbations resulted in similar gain and phase response for both pivots below 3 Hz. Higher frequencies show a higher gain together with an increasing phase lag up to 180° for the upper pivot with respect to the lower pivot. For frequencies below 3 Hz increasing the perturbation level resulted in a significant relative lower neck deformation increase ($P < 0.05$) against a major decrease of relative upper neck deformations ($P < 0.001$). Above 3 Hz both pivots showed similar responses as the low perturbation levels. These results suggest different muscle activity strategies by adapting to the stimulus for the upper and lower neck during neck stabilization below 3 Hz, while the frequency responses above 3 Hz seem to be dominated by inertia and passive resistance.

Neck bending has two different shapes: (1) C-shaped neck bending is realized when the upper and lower neck bend in the same direction, and (2) S-shaped neck bending is a result of bending in different directions in the upper and lower neck. Comparable phase characteristics as found up to approximately 3 Hz for both pivots suggests C-shaped neck bending. The 180° phase lag for frequencies above approximately 5 Hz indicates S-shaped neck bending.

Mental arithmetic and exclusion of visual feedback resulted in significantly increasing neck rotations between 0.8-7 Hz for the upper pivot. The lower pivot showed a decrease during

mental distraction between 0.8-3 Hz and a increase during visual feedback exclusion between 3-7 Hz.

The frequency response functions shown for head motion as well as for pivot rotations gave a lot of information on the physical responses, however detailed stabilizing reflexes could not be described. Therefore, the parametric identification of a neuromuscular neck model was started, however not completed and presented in this paper.

Publication

It is proposed to submit this paper the Journal of Biomechanics. The number of words and figures shall be reduced to the compulsory length of 3000 words for submission. Appendix A (and crossreferences) will be omitted, while Appendix B & C will be shortened. Keshner should be contacted for approval of Figure 7. The current content of the paper is expected to be sufficient for submission, however if needed a parametric identification should be performed.

References

Cenciarini, M., Peterka, R., 2006. Stimulus–dependent changes in the vestibular contribution to human postural control. Journal of Neurophysiology 95, 2733–2750.

Clauser, C., McConville, J., Young, J., 1969. Weight, volume, and center of mass of segments of the human body. Tech. rep., Aerospace Medical Research Laboratories, Wright-Patterson Air Force Base, OH.

de Vlugt, E., Schouten, A., van der Helm, F., 2006. Quantification of intrinsic and reflexive properties during multijoint arm posture. Journal of Neuroscience Methods 155, 328–349.

Fard, M., Ishihara, T., Inooka, H., 2004. Identification of the head–neck complex in response to trunk horizontal vibration. Biological Cybernetics 90, 418–426.

Guitton, D., Kearney, R., Wereley, N., Peterson, B., 1986. Visual, vestibular and voluntary contributions to human head stabilization. Experimental Brain Research 64, 59–69.

Happee, R., van Drunen, P., 2009. Posture maintenance of the human neck. Digital Human Modeling for Design and Engineering Conference and Exhibition, Society of Automotive Engineers,Gothenburg, 1–6.

Keshner, E., 2000. Modulating active stiffness affects head stabilizing strategies in young and elderly adults during trunk rotations in the vertical plane. Gait and Posture 11, 1–11.

Keshner, E., 2003. Head-trunk coordination during linear anterior-posterior translations. Journal of Neurophysiologics 89, 1891–1901.

Keshner, E., Kenyon, R., Langston, J., 2004. Postural responses exhibit multisensory dependencies with discordant visual and support surface motion. Journal of Vestibular Research 14, 307–319.

Mugge, W., Abbink, D., van der Helm, F., 2007. Reduced power method: how to evoke low-bandwidth behaviour while estimating full-bandwidth dynamics. In: Rehabilitation Robotics, 2007. ICORR 2007. IEEE 10th International Conference on. pp. 575–581.

Ono, K., Ejima, S., Suzuki, Y., Kaneoka, K., Fukushima, M., Ujihashi, S., 2006. Prediction of neck injury risk based on the analysis of localized cervical vertebral motion of human volunteers during low–speed rear impacts. IRCOBI Conference, 103–113.

Pedrocchi, A., Ferrigno, G., 2004. Model of head–neck joint fast movements in the frontal plane. Biological Cybernetics 90, 377–389.

Peng, G., 1996. Dynamics and control of head, neck and eye stabilization: Neuromechanical and experimental models. Ph.D. thesis, Northwestern University Evanston, IL.

Peterka, R., 2002. Sensorimotor integration in human postural control. Journal of Neurophysiological 88, 1097–1118.

Plaga, J., Albery, C., Boehmer, M., Goodyear, C., Thomas, G., 2005. Design and development of anthropometrcially correct head forms for joint strike fighter ejection seat testing. Wright-PattersonsAFB, 56.

Schouten, A., de Vlugt, E., van Hilten, J., van der Helm, F., 2008. Quantifying proprioceptive reflexes during position control of the human arm. IEEE Transactions on Medical Engineering 55, 311–321.

Simoneau, M., Denninger, M., Hain, T., 2008. Role of loading on the head stability and effective neck stiffness and viscosity. Journal of Biomechanics.

Tangorra, J., Jones, L., Hunter, I., 2003. Dynamics of the human head-neck system in the horizontal plane: Joint properties with respect to a static torque. Annals of Biomedical Engineering 31 (5), 606–620.

van der Helm, F., Schouten, A., de Vlugt, E., Brouwn, G., 2002. Identification of intrinsic and reflexive components of human arm dynamics during postural control. Journal of Neuroscience Methods 119, 1–14.

van der Horst, M., 2002. Human head neck response in frontal, lateral and rear end impact loading: modeling and validation. Ph.D. thesis, Technical University Eindhoven.

Vuillerme, N., Vincent, H., 2006. How performing a mental arithmetic task modify the regulation of center of foot pressure displacements during bipedal quiet standing. Experimental Brain Research 169, 130–134.

Wismans, J., Philippens, M., van Oorschot, E., Kallieris, D., Mattern, R., 1987. Comparison of human volunteer and cadaver head-neck response in frontal flexion. Proceedings of the Thirty-First Stapp Car Crash Conference, Society of Automotive Engineers, Warrendale, 1–11.

A Platform Dynamics and Motion Capture versus Accelerometers

Figure 2 shows differences between the designed disturbance and the actual applied disturbance at the incisura jugularis (IJ). In this Appendix an explanation is given. Also the Xsens and motion capture data is evaluated and compared.

1.1. Platform dynamics

When evaluating the difference between the designed disturbance and the actual applied disturbance three in-between systems should be analyzed: The response of the platform to the designed perturbation (Figure 9(a)), the platform to chair transmission (Figure 9(b)) and the transfer between the chair and IJ (Figure 10).

During the experiments the hydraulic pistons of the motion platform motion were restricted by a rate limiter and a saturation at 0.25 m/s and 0.14 m. Therefore, the response of the platform to the designed perturbation showed a good response up to 1 Hz but did not replicate the designed perturbation at higher frequencies. Obviously these effects were not planned and therefore recommended as an adjustment to future experiments.

The coupling of the chair to the platform showed good results up to 2 Hz. However, at frequency higher than 2 Hz an increase in gain is found, indicating that the chair is not as rigid as claimed. So an increase in chair stiffness will substantially increase the transfer of the designed perturbation and the actual IJ disturbance and is therefore also recommended.

The chair to IJ acceleration transfer shows very good results, indicating the seat to body contact and seat belt restriction are sufficient. Low underdamped behavior around 4 Hz is easily explained by the human dynamics, representing connection between the chair and back and the thorax tissue.

However, despite the deficiencies in the transfer of the designed disturbance to the actual applied IJ disturbance, the experimental data is still very useful for data analysis. The signal-to-noise ratio is good for frequencies up till approximately 12 Hz, since the coherence of all three in-between systems were still high.

1.2. Motion capture versus accelerometers

Comparison of the motion capture (MoCap) data and the accelerometer (Xsens) data will provide information of the accuracy of both systems with respect to each other. Therefore, the FRFs between the chair and IJ for both the double differentiated Mocap data ($\hat{H}_{\ddot{X}_{CH},\ddot{X}_{IJ}}$) and the Xsens ($\hat{H}_{A_{CH},A_{IJ}}$) data is given, as well as the FRFs between the MoCap and Xsens data of the chair ($\hat{H}_{\ddot{X}_{CH},A_{CH}}$) and IJ ($\hat{H}_{\ddot{X}_{IJ},A_{IJ}}$).

Comparing the chair to IJ FRFs from the MoCap and the Xsens show very similar responses except for frequencies below 1 Hz (Figure 10). The Xsens data show a drop in gain and coherence at low frequencies, possibly explained by respiratory motion of the thorax (regular respiration is within the range of 10-18 times per minute with a time period of two seconds) and low signal-to-noise ratio for accelerometers at low frequencies. Since the respiratory motion are small movements, they were not measured by the motion capture due to the accuracy of the system.

The difference in measurements at the chair and IJ between the two measurement systems show comparable results up to 4 Hz (Figure 11). Then the Xsens data drops a little with respect to the motion capture. The cause could be a (4 Hz) low-pass filter at the Xsens. For the IJ measurements also the difference in the low frequencies are found again.

Concluding the double differentiated MoCap data and the Xsens data were similar, except for the noisy behavior at low frequencies of the Xsens data. Optimally the recorded MoCap and Xsens data could be merged using a Kalman filter, however due to the high similarity level no big improvements were expected. Therefore, only the MoCap data was analyzed in this study.

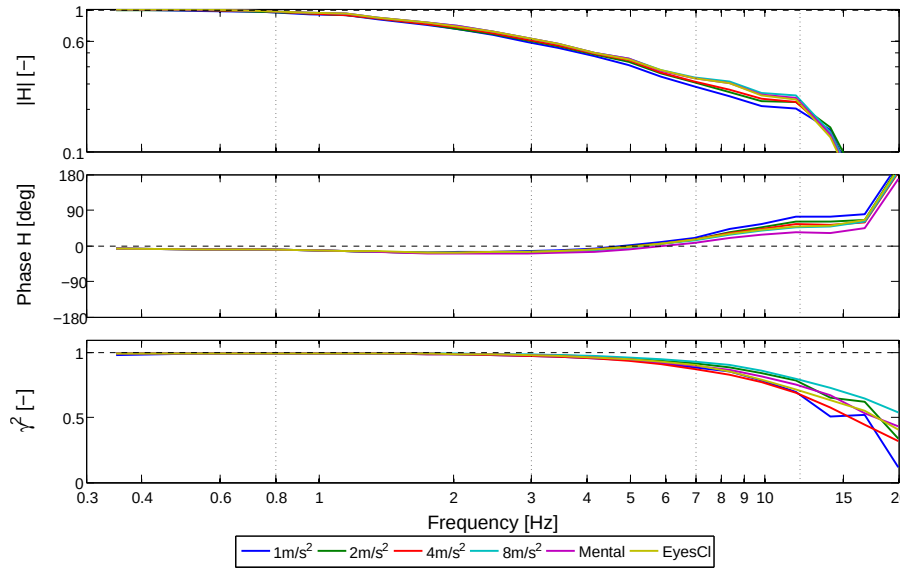

((a))

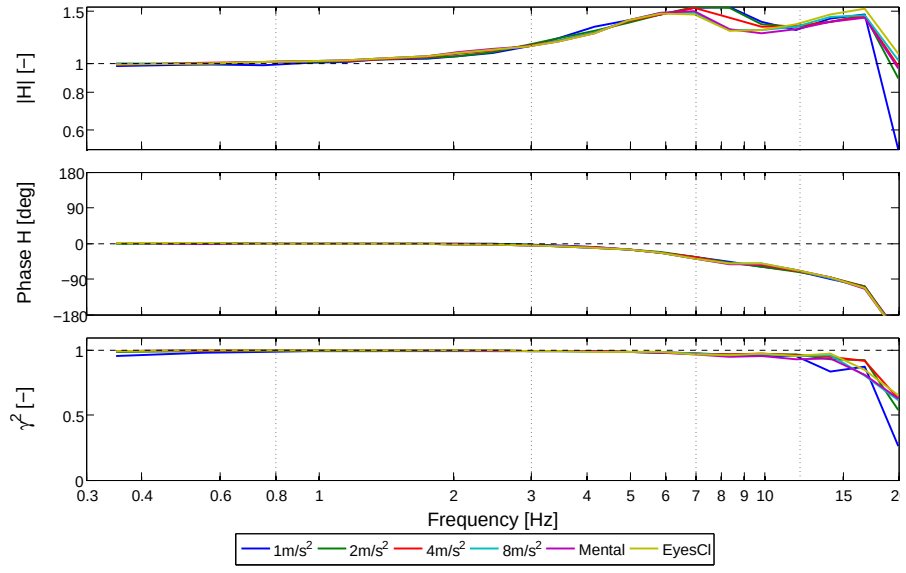

((b))

Figure 9: *Gain, Phase & Squared Coherence of platform and chair dynamics. All six different conditions ($1m/s^2$, $2m/s^2$, $4m/s^2$, $8m/s^2$, Mental Arithmetic & Eyes Closed) are shown. The four different frequency ranges are marked by the vertical dotted lines.*
a: $\hat{H}_{\ddot{D},A_{PL}}$, Transfer for designed disturbance accelerations ($\ddot{D}$) to horizontal platform Xsens accelerations (A_{PL})
b: $\hat{H}_{A_{PL},A_{CH}}$, Transfer for horizontal platform Xsens accelerations (A_{PL}) to horizontal chair Xsens accelerations (A_{CH})

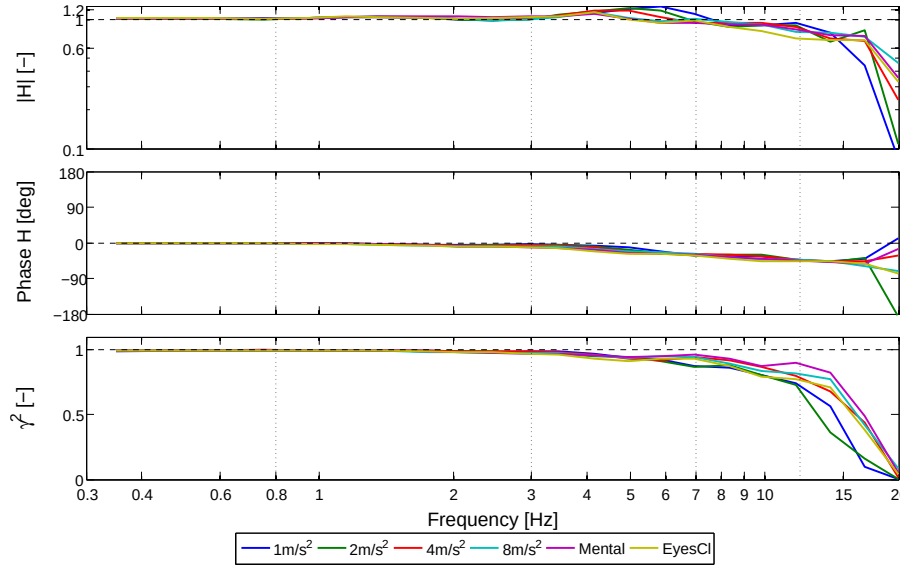

((a))

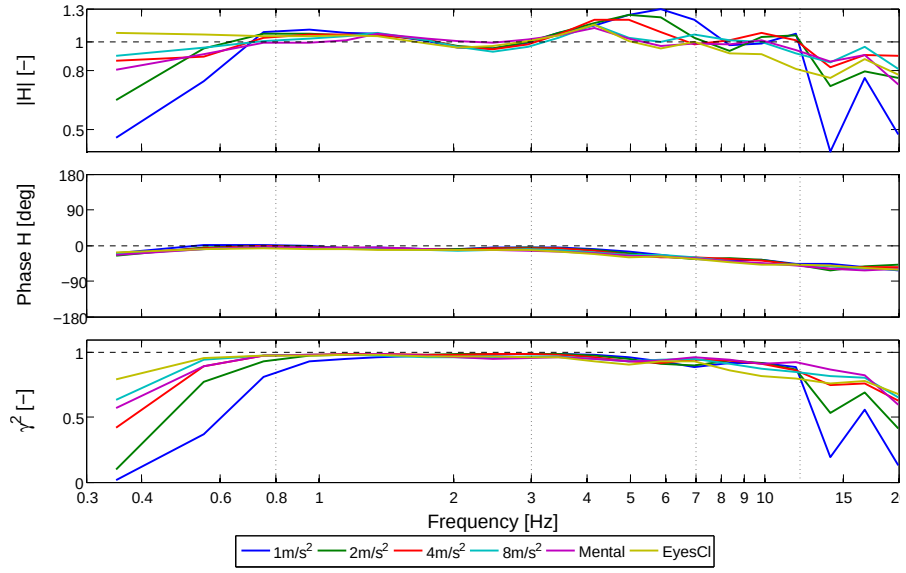

((b))

Figure 10: *Gain, Phase & Squared Coherence of thorax dynamics from both the motion capture (MoCap) and the accelerometer data (Xsens). All six different conditions ($1m/s^2$, $2m/s^2$, $4m/s^2$, $8m/s^2$, Mental Arithmetic & Eyes Closed) are shown. The four different frequency ranges are marked by the vertical dotted lines.*
a: $\hat{H}_{\ddot{X}_{CH},\ddot{X}_{IJ}}$, Transfer of the double derivative of Mocap for the horizontal chair accelerations to the horizontal incisura jugularis accelerations
b: $\hat{H}_{A_{CH},A_{IJ}}$, Transfer of the Xsens horizontal chair accelerations to the horizontal incisura jugularis accelerations

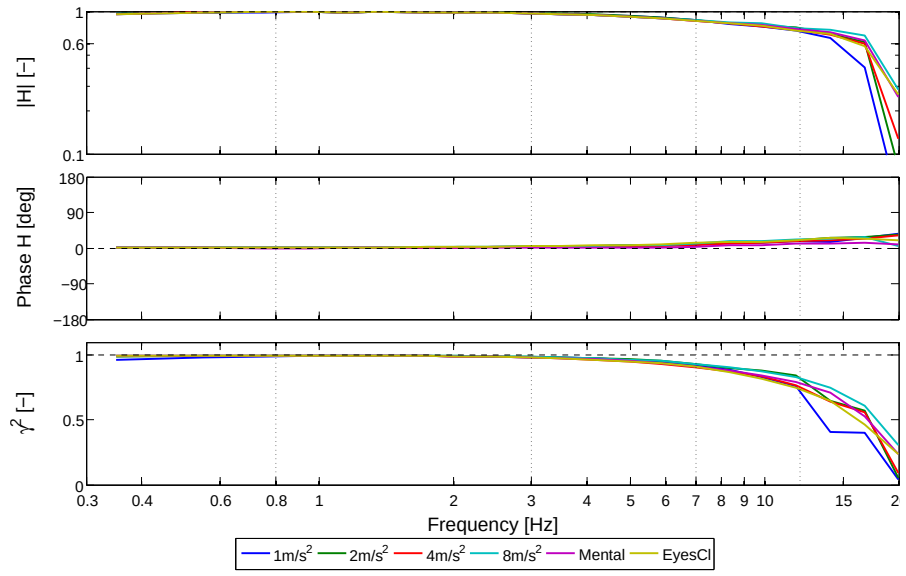

((a))

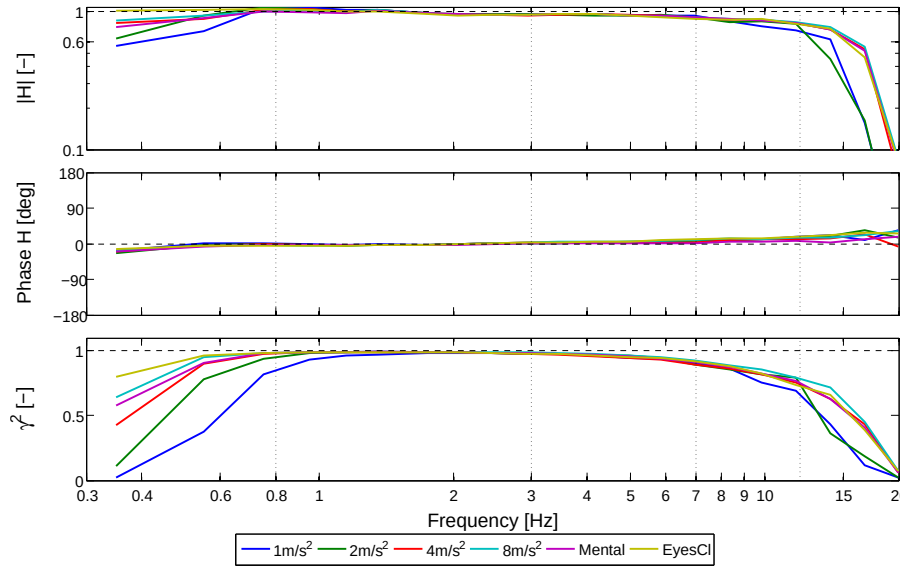

((b))

Figure 11: *Gain, Phase & Squared Coherence for comparison of the double derivative of motion capture data ($\ddot{X}$)to the accelerometer data (A) at the chair (CH) and incisura jugularis (IJ). All six different conditions ($1m/s^2$, $2m/s^2$, $4m/s^2$, $8m/s^2$, Mental Arithmetic & Eyes Closed) are shown. The four different frequency ranges are marked by the vertical dotted lines.*
a: $\hat{H}_{\ddot{X}_{CH},A_{CH}}$, Transfer for motion capture data to the accelerometer data both of the chair
b: $\hat{H}_{\ddot{X}_{IJ},A_{IJ}}$, Transfer for motion capture data to the accelerometer data both of the incisura jugularis

B Nonparametric plots

To check if the horizontal perturbation does not result in unexpected big vertical head perturbation the gain, phase and coherence characteristics are shown (Figure 12(a)). While the human neck bends during the experiments some vertical displacement is expected. Up till 4 Hz the vertical head displacement show low gain (< 0.2). Above 4 Hz the gain increases slightly to 0.7, however, due to the low perturbation power at these frequencies the vertical motion is still small enough. Concluding the vertical head displacements are small as expected.

Figure 12(b) shows the FRF between the incisura jugularis disturbance and the horizontal temple-IJ (local head) displacements and can be compared with global head displacements (Figure 5(a)). This figure is a good representation of the neck dynamics in horizontal direction and shows low gain in the low frequencies with a phase lag of 90$\circ$, resulting in almost similar motion as IJ. Between 1.5-5 Hz head displacements were bigger than the perturbation with a phase lag shifting from $90 - 180^{\circ}$. Above 5 Hz a gain of approximately one was found with a phase lag of 180°, representing motion of the head in opposite direction of the IJ disturbance resulting in allmost no motion of the head. The FRF of the local horizontal head displacements is as expected much more similar to the pivot rotation FRFs than the global horizontal head displacements.

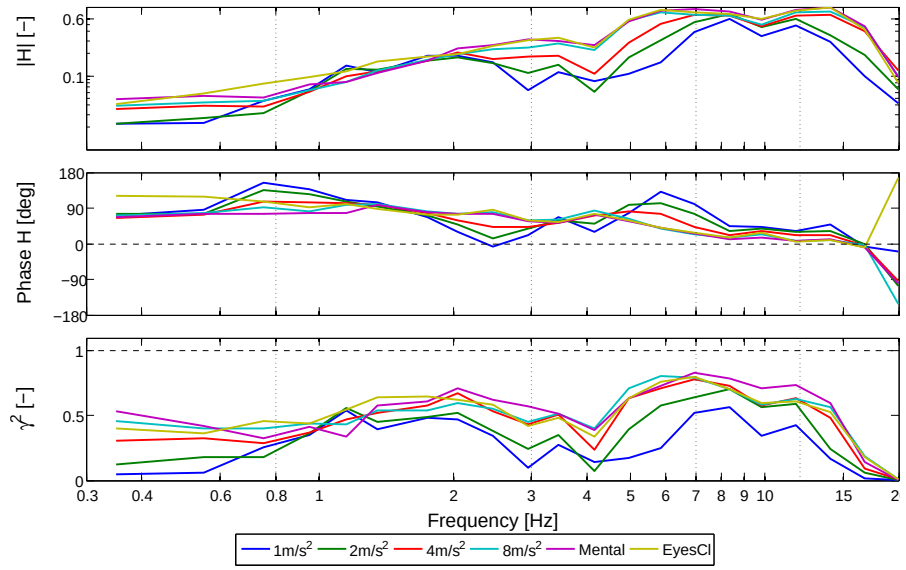

((a))

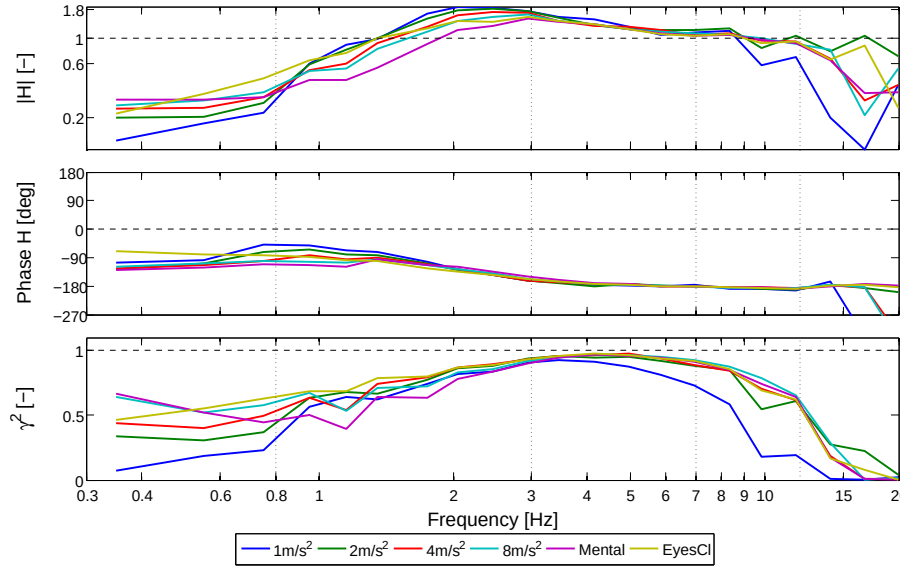

((b))

Figure 12: *Gain, Phase & Squared Coherence of the global head vertical displacement (Z_{TP}) with respect to the horizontal incisura jugularis displacements (X_{IJ}). All six different conditions ($1m/s^2$, $2m/s^2$, $4m/s^2$, $8m/s^2$, Mental Arithmetic & Eyes Closed) are shown. The four different frequency ranges are marked by the vertical dotted lines.*
a: $\hat{H}_{Z_{TP}}$, Transfer for horizontal incisura jugularis disturbance to vertical temple (head) displacements
b: $\hat{H}_{X_{TP}-X_{IJ}}$, Transfer for horizontal incisura jugularis disturbance to "horizontal temple - horizontal incisura jugularis" (local head) displacements

C Results Students T-test

In section 4.2. the significant mean value differences of the gain for the FRFs of the horizontal head translation ($H_{X_{TP}}$), head rotation (H_{α}), lower pivot rotation ($H_{\phi_{LP}}$), and upper pivot rotation ($H_{\phi_{UP}}$) (Figure 5 & 6) are discussed. Detailed results of the two-tailed two-paired Student T-test (p-values) for the gain, phase and coherence characteristics are shown in Table 5.

For the horizontal head displacement, head rotations and the lower pivot angles a significant pattern of decrease in perturbation level resulting in a decrease of coherence is found. This is expected while the signal-to-noise ratio decreases for a decrease in perturbation level. However, the upper pivot angle has an increase of coherence between 0.8 and 7 Hz for decreasing perturbation levels. Mental distraction and covering of the eyes was used for an increase in the lower frequency levels. But after evaluation no significant increase is found for the horizontal head displacement and head rotations (even small decreases). However, a significant coherence increase is found between 3-7 Hz for the lower pivot and between 0.8-7 Hz for the upper pivot.

For discussion of the gain characteristics see Section 4.2. The phase characteristics show sometimes very messy results. Therefore, the significance of the phase has less value than the gain and coherence significances.

Table 5
P-values and mean value differences of the gain, phase and coherence characteristics for the FRFs between incisura jugularis horizontal displacement to the horizontal head displacement, the head angle, the lower pivot angle and the upper pivot angle (from left to right). The FRFs from all conditions ([1;2;4] m/s^2, Mental Arithmetic & Eyes Closed) are compared with the FRF of the $8m/s^2$-condition within the four different frequency ranges. Significant values are bold.

			|H|: X_{TP}				**|H|: α**				**|H|: Φ_{LP}**				**|H|: Φ_{UP}**			
			0-0.8 Hz	**0.8-3 Hz**	**3-7 Hz**	**7-12 Hz**	**0-0.8 Hz**	**0.8-3 Hz**	**3-7 Hz**	**7-12 Hz**	**0-0.8 Hz**	**0.8-3 Hz**	**3-7 Hz**	**7-12 Hz**	**0-0.8 Hz**	**0.8-3 Hz**	**3-7 Hz**	**7-12 Hz**
1 m/s²	**p**	**[-]**	**5.8E-06**	**8.2E-24**	**1.2E-05**	**2.0E-04**	2.5E-01	**6.1E-21**	**4.4E-15**	**1.0E-05**	**2.7E-04**	**4.1E-02**	**2.1E-02**	2.4E-01	**2.2E-16**	**2.8E-32**	**1.4E-05**	1.9E-01
	av	**[-]**	**1.099**	**1.341**	**1.311**	**1.727**	0.938	**1.471**	**1.206**	**1.205**	**0.764**	**0.918**	**0.867**	0.955	**2.354**	**2.342**	**1.330**	1.050
2 m/s²	**p**	**[-]**	**4.4E-02**	**5.3E-13**	**2.5E-02**	**3.6E-03**	7.3E-01	**4.6E-15**	**1.1E-17**	**1.7E-02**	**4.5E-05**	**1.9E-02**	9.5E-01	5.9E-01	**1.7E-09**	**7.0E-22**	**2.6E-07**	6.3E-01
	av	**[-]**	**1.044**	**1.223**	**1.151**	**1.370**	0.981	**1.376**	**1.201**	**1.090**	**0.770**	**0.908**	0.997	0.982	**1.729**	**2.095**	**1.373**	1.015
4 m/s²	**p**	**[-]**	5.8E-01	**4.3E-03**	7.5E-01	6.6E-01	6.9E-01	**1.2E-04**	**3.9E-11**	3.2E-01	**3.9E-03**	**3.5E-02**	5.9E-01	8.9E-02	**4.7E-03**	**2.3E-07**	**1.2E-04**	1.1E-01
	av	**[-]**	0.990	**1.082**	1.020	1.041	1.020	**1.174**	**1.133**	1.039	**0.833**	**0.916**	1.030	1.054	**1.258**	**1.487**	**1.269**	1.051
Mental Arithmetic	**p**	**[-]**	**1.1E-03**	**5.1E-04**	4.0E-01	6.0E-01	4.4E-01	**2.5E-03**	7.1E-01	1.7E-01	9.7E-01	**7.9E-06**	7.3E-02	2.3E-01	3.6E-01	**1.8E-02**	5.9E-01	5.2E-02
	av	**[-]**	**0.944**	**0.901**	1.057	1.050	1.043	**0.875**	0.993	0.953	0.997	**0.810**	1.094	0.964	1.079	**1.209**	1.037	0.944
Eyes Closed	**p**	**[-]**	**6.2E-20**	3.6E-01	4.8E-01	1.6E-01	**6.8E-03**	**1.4E-02**	8.8E-02	3.9E-01	7.5E-01	3.4E-01	**3.7E-02**	3.5E-01	6.1E-02	**4.9E-04**	**1.4E-02**	5.5E-01
	av	**[-]**	**1.172**	0.975	0.957	0.882	**1.159**	**1.100**	1.032	0.968	1.021	0.963	**1.121**	1.026	1.189	**1.352**	**1.176**	1.017

			Phase H: X_{TP}				**Phase H: α**				**Phase H: Φ_{LP}**				**Phase H: Φ_{UP}**			
			0-0.8 Hz	**0.8-3 Hz**	**3-7 Hz**	**7-12 Hz**	**0-0.8 Hz**	**0.8-3 Hz**	**3-7 Hz**	**7-12 Hz**	**0-0.8 Hz**	**0.8-3 Hz**	**3-7 Hz**	**7-12 Hz**	**0-0.8 Hz**	**0.8-3 Hz**	**3-7 Hz**	**7-12 Hz**
1 m/s²	**p**	**[-]**	**7.5E-15**	1.2E-01	8.3E-02	6.2E-01	8.2E-02	**4.6E-08**	**2.3E-03**	**8.4E-06**	**2.7E-03**	**5.5E-07**	**3.1E-04**	**5.0E-05**	**6.8E-03**	**6.5E-24**	**8.5E-06**	**8.5E-04**
	av	**[-]**	**0.518**	1.083	0.665	1.155	1.167	**1.316**	**0.596**	**0.779**	**0.621**	**1.252**	**1.395**	**1.546**	**2.433**	**11.764**	**0.596**	**0.833**
2 m/s²	**p**	**[-]**	**8.7E-07**	7.7E-02	2.5E-01	8.9E-02	2.1E-01	**5.0E-04**	6.1E-01	**2.8E-03**	3.4E-01	**9.2E-05**	**2.7E-04**	6.2E-02	**2.6E-02**	**6.7E-18**	7.8E-01	2.8E-01
	av	**[-]**	**0.709**	1.094	0.773	1.543	1.090	**1.182**	1.073	**0.881**	0.910	**1.176**	**1.363**	1.196	**2.081**	**9.827**	0.973	0.952
4 m/s²	**p**	**[-]**	8.8E-02	2.6E-01	3.8E-01	5.0E-01	9.3E-01	7.4E-02	1.9E-01	7.6E-01	4.7E-01	7.5E-02	7.0E-02	6.8E-01	**1.3E-02**	**5.4E-11**	5.9E-01	3.2E-01
	av	**[-]**	0.899	1.056	1.162	0.784	1.004	1.080	1.196	0.989	0.958	1.075	1.192	1.039	**2.192**	**7.463**	1.054	1.043
Mental Arithmetic	**p**	**[-]**	9.3E-01	**1.6E-04**	4.8E-01	4.0E-01	**2.1E-03**	2.0E-01	5.5E-01	8.5E-01	**1.4E-02**	1.0E+00	**7.1E-03**	6.3E-01	7.1E-01	6.0E-01	6.6E-02	4.6E-01
	av	**[-]**	0.994	**0.832**	1.126	0.735	**0.863**	0.948	1.085	1.007	**0.863**	1.000	**1.259**	0.956	1.172	0.448	1.203	1.035
Eyes Closed	**p**	**[-]**	6.8E-01	9.5E-02	5.3E-01	7.7E-01	**1.2E-18**	9.5E-01	**1.9E-02**	5.9E-01	**1.7E-13**	**3.6E-02**	**2.7E-03**	7.8E-01	**5.4E-04**	**2.5E-02**	**2.1E-03**	1.5E-01
	av	**[-]**	0.975	1.077	0.882	0.910	**1.421**	0.998	**1.351**	0.973	**1.367**	**0.894**	**1.284**	0.972	**2.757**	**3.544**	**1.306**	0.903

			γ^2: X_{TP}				**γ^2: α**				**γ^2: Φ_{LP}**				**γ^2: Φ_{UP}**			
			0-0.8 Hz	**0.8-3 Hz**	**3-7 Hz**	**7-12 Hz**	**0-0.8 Hz**	**0.8-3 Hz**	**3-7 Hz**	**7-12 Hz**	**0-0.8 Hz**	**0.8-3 Hz**	**3-7 Hz**	**7-12 Hz**	**0-0.8 Hz**	**0.8-3 Hz**	**3-7 Hz**	**7-12 Hz**
1 m/s²	**p**	**[-]**	**3.3E-06**	**1.1E-02**	2.2E-01	2.2E-01	**6.0E-24**	**1.2E-03**	**1.7E-04**	**1.4E-09**	**4.8E-31**	**2.7E-08**	**5.2E-06**	**1.7E-08**	**2.0E-04**	**5.9E-09**	6.5E-01	**1.1E-10**
	av	**[-]**	**0.949**	**0.977**	0.948	0.886	**0.617**	**0.963**	**0.974**	**0.858**	**0.457**	**0.914**	**0.906**	**0.893**	**0.747**	**1.204**	1.006	**0.880**
2 m/s²	**p**	**[-]**	**5.0E-03**	1.0E-01	4.4E-01	8.3E-01	**3.5E-12**	8.2E-01	9.7E-01	**2.2E-03**	**1.8E-10**	7.8E-01	6.8E-01	**1.1E-02**	1.1E-01	**2.8E-10**	**6.3E-06**	**1.0E-04**
	av	**[-]**	**0.979**	1.011	1.030	0.981	**0.755**	0.998	1.000	**0.941**	**0.709**	0.997	0.994	**0.963**	0.887	**1.223**	**1.047**	**0.946**
4 m/s²	**p**	**[-]**	**2.3E-03**	5.2E-01	9.1E-01	3.3E-01	**1.7E-06**	3.1E-01	7.0E-01	1.6E-01	**7.3E-06**	5.7E-01	3.3E-01	5.3E-01	7.0E-01	**2.6E-06**	**4.1E-05**	5.9E-01
	av	**[-]**	**0.979**	1.005	0.995	0.913	**0.844**	0.988	1.001	0.976	**0.806**	0.993	1.014	1.006	0.973	**1.171**	**1.045**	0.995
Mental Arithmetic	**p**	**[-]**	2.6E-01	1.8E-01	8.3E-01	5.5E-01	3.5E-01	**2.2E-02**	8.1E-01	7.8E-01	6.2E-01	**8.3E-04**	**5.0E-03**	6.1E-02	5.0E-01	**2.0E-04**	**4.3E-02**	3.2E-01
	av	**[-]**	0.992	0.986	1.009	1.053	0.970	**0.969**	1.001	0.996	1.022	**0.946**	**1.036**	1.015	0.953	**1.137**	**1.023**	1.006
Eyes Closed	**p**	**[-]**	8.9E-01	7.5E-02	7.8E-01	4.3E-01	**4.8E-02**	6.9E-02	9.3E-01	**3.5E-02**	9.1E-01	4.7E-01	**2.4E-02**	5.5E-01	2.5E-01	**3.2E-04**	**8.8E-04**	5.8E-01
	av	**[-]**	1.001	0.983	0.988	0.927	**0.940**	1.019	1.000	**0.965**	1.005	1.009	**1.030**	1.005	1.080	**1.132**	**1.035**	0.996